Proceedings of the 21st ICSMGE, Vienna, Austria, 14 – 19 June 2026. Pistrol, Adam & Schweiger (eds.)
Published by: ÖGG, Austrian Society for Geomechanics, Salzburg, Austria, ISBN 978-3-9503898-4-5
https://doi.org/10.53243/ICSMGE2026-2356

Fundamental Investigation of detecting underground cavities with seismic wave survey based on a homogeneous ground model with laboratory scale testing

Yutaro Hara
Department of Covil Engineering, Graduate School of Engineering, The University of Tokyo, Tokyo, Japan, yutarohara13579@g.ecc.u-tokyo.ac.jp

Reiko Kuwano
Institution of Industrial Science, The University of Tokyo, Tokyo, Japan

ABSTRACT: Non-destructive detection of underground cavities is critical to preventing catastrophic ground sinkholes that can paralyze transportation networks and rupture lifeline infrastructure. Conventional ground-penetrating radar rarely images deeper than ~2 m, leaving a diagnostic gap for cavities buried at greater depths. This study evaluates elastic-wave prospecting as a supplemental technique by conducting controlled laboratory experiments in a large, vibration-isolated sand box that replicates near-surface conditions while eliminating field noise. A homogeneous dry silica sand ground model (D_{50} = 0.5 mm; ρ_d = 1.46 g / cm³) of 450 mm thick was prepared by air pluviation. A polycarbonate rectangular cavity (120 mm × 60 mm × 450 mm) was embedded 110 mm beneath the surface. Vertically polarized waves were generated by a steel-ball drop pulse source (dominant frequency ≈ 400 Hz) and recorded at 100 kHz by ADXL354 accelerometers. Waveforms for cavity-bearing and reference (homogeneous) cases were compared. Cross-correlation with the source signature isolated direct, reflected, and refracted arrivals; Fourier spectra revealed frequency-dependent attenuation. Dispersion images computed with the frequency and phase velocity transform identified three diagnostic signatures of the cavity: (1) persistent reflected and refracted energy between the source and cavity, visible as local spectral peaks; (2) an additional high-frequency (> 500 Hz) dispersion branch attributed to a guided mode confined between the ground surface and cavity roof; and (3) enhanced geometric spreading and rapid decay of direct-wave amplitudes directly above the cavity, evidencing energy leakage into guided waves. The 1/10-scale results demonstrate that elastic-wave methods can resolve cavities far deeper than the practical GPR limit and provide multiple independent indicators—arrival pattern, dispersion anomaly, and amplitude decay—for robust detection. These findings advance seismic monitoring as a viable countermeasure against deep underground cavities and the ground sinkholes.

KEYWORDS: underground cavity, model test, seismic wave.

1 INTRODUCTION

Non-destructive detection of underground cavities has become an urgent issue in the mitigation of ground sinkholes. Because such cavities can trigger sudden subsidence that severely damages roadways and buried utilities—and may even threaten human life—early identification while remediation is still feasible is essential by Kuwano (2009). Although relatively large sinkholes originating from cavities at depths of ~10 m have been reported, ground-penetrating radar (GPR), the most common geophysical tool for cavity detection, can generally image features only to ~2 m depth. Consequently, the present study focuses on using seismic (elastic-wave) prospecting to detect cavities deeper than 2 m.

Soils are particulate granular media and exhibit complex behaviors—including inelastic attenuation—that differ markedly from ideal elastic solids. Numerical studies employing the discrete-element method (DEM) have suggested that reflections from cavities may be observable, yet field verification has been inconclusive because heterogeneous near-surface conditions obscure the seismic response of cavities (Kuwashiro; Karasaki). To isolate cavity effects, we conducted elastic-wave experiments on a homogeneous model ground in which material properties and density were tightly controlled. A large, vibration-isolated sand box was constructed to record elastic-wave propagation free from external noise. A 1/10-scale seismic survey was simulated to capture wavefields generated when a cavity is present in granular soil. Two cases—homogeneous ground and cavity-bearing ground—were compared in terms of: (i) reflection and refraction arrivals, (ii) surface-wave dispersion, and (iii) attenuation characteristics, thereby evaluating how underground cavities modify near-surface elastic-wave propagation.

2 WAVE PROPAGATION MEASUREMENTS IN THE MODEL GROUND

2.1 *Experimental Sand Box, Ground Materials, and Test Procedures*

Figure 1 outlines the experimental setup. The fabricated sand box measures 520 mm (W) × 450 mm (H) × 930 mm (L); anti-vibration rubber pads isolate both the box and its support frame, and urethane foam suppresses wall reflections. Homogeneous dry silica sand No. 6 was pluviated to form the model ground. Key material parameters are listed in Table 1.

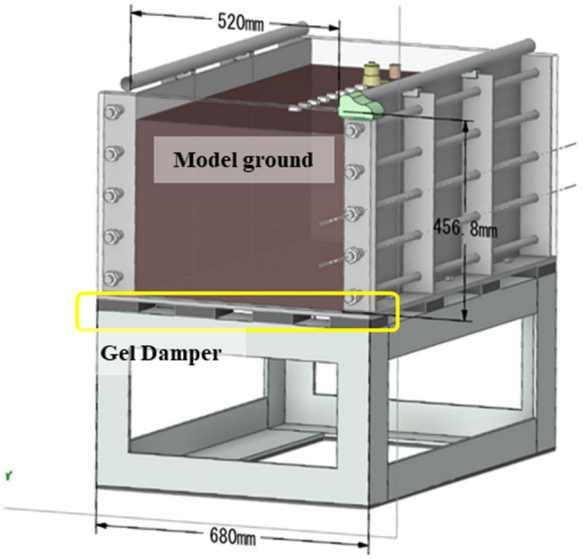

Figure 1. Overview of experimental sandbox.

Table 1. Physical properties of the model ground material

50% grainsize $D_{50}[mm]$	Dry density $\rho_d[g/cm^3]$	Water content W_c [%]	Voil ratio e
0.5	1.46	0	0.81

A rectangular cavity measuring 120 mm (W) × 60 mm (H) × 450 mm (L), as shown in Figure (2a), was built from polycarbonate panels and embedded. The position was shown in Figure (2b). The seismic source was a steel-ball drop pulse sensor in Figure (2c); Tao (2019), with a dominant frequency of 400 Hz. Vertical ground motion was recorded by Analog Devices MEMS triaxial accelerometers (ADXL354); Figure (2d) pressed against the ground surface under static load. A Keyence NR600 data logger sampled 100 kHz for 30 000 samples. For both homogeneous and cavity cases the measured shear-wave velocity V_s was approximately 43.0 m/s.

2.2 *Analysis Method*

2.2.1 *Extraction of Cavity Reflections and Dispersion Characteristics*

Recorded traces were cross-correlated with the previously measured source signature Equation (1) to separate direct, reflected, and refracted arrivals from underground cavities.

$$C_{SR}[\tau] = \sum_{t=1}^{T} S[t]R[t+\tau] \tag{1}$$

Where $C_{SR}[t]$, $S[t]$, $R[t]$ is Cross-correlation, source, and receiver signals in time step difference τ, respectively.

Because vertical motion was monitored, Rayleigh waves dominated the surface-wave field. Dispersion $V(c,\omega)$ was calculated with the ω–c (phase-velocity) transform of Park et al. as shown in Equation (2) below:

$$\begin{cases} V(\omega,\ c\ ) = \sum_{x=x_0}^{Nx} e^{icx} \dfrac{U(x,\omega)}{|U(x,\omega)|} \\ U(x,\omega) = \sum_{t=0}^{Nt} e^{i\omega t} u(x,t)\Delta t \end{cases} \tag{2}$$

here c denotes phase velocity at its first appearance with x the source–receiver offset, sampling tine interval $\Delta t = 10\mu s$, and $U(x,\omega)$ is the discrete Fourier transform of the time-domain record $u(x,t)$. Nx is the number of receivers, and Nt is the length of the signal.

2.2.2 Attenuation Characteristics

Amplitude spectra were extracted from mixed direct-plus-reflected windows (direct wave ≈ 0–0.03 s; mixed wave 0–0.06 s) and plotted against propagation distance. Representative spectra are shown in Figure (3). The amplitude W_a of a wace of frequency f after traveling distance R_a is expressed by Bornitz Equation (3):

$$W_a = W_0 \times \left[\frac{R_a}{R_0}\right]^{-n} \times e^{\alpha f(R_a - R_0)} \tag{3}$$

Where W_0 is the amplitude at R_0 , n the geometrical-spreading exponent, and α the material-damping coefficient. For Rayleigh waves on a planar surface $n = 0.5$. With $\alpha \approx 1.2 \times 10^{-3}\ s/m$, material damping was negligible relative to geometric spreading, so direct-wave amplitude decayed quasi-linearly on logarithmic axes. Least-squares fitting yielded n and the 1 m reference spectrum A_0.

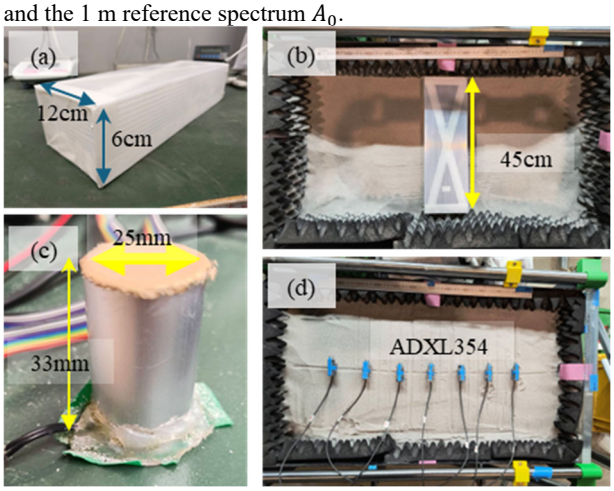

Figure 2. (a) Simulated cavity, (b) Cavity arrangement in the cavity ground, (c) Steel ball drop-type vibration generator[4], (d) Receiver arrangement on the sand box surface.

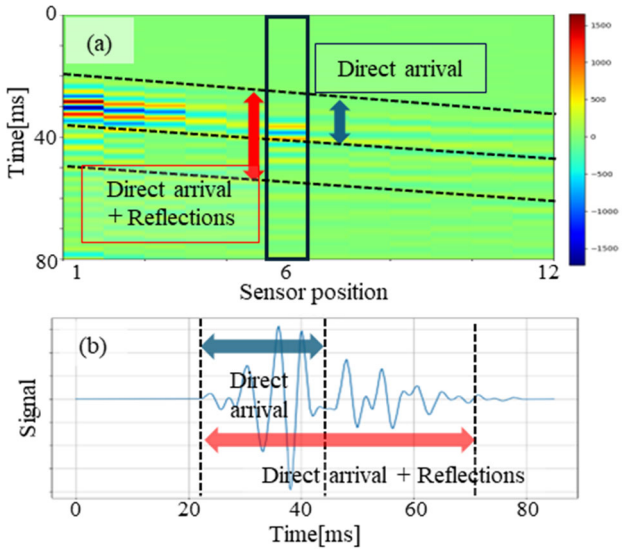

Figure 3. Examples of extracting the direct wave and the direct–reflected mixed wave: (a) entire waveform; (b) waveform recorded at the receiver.

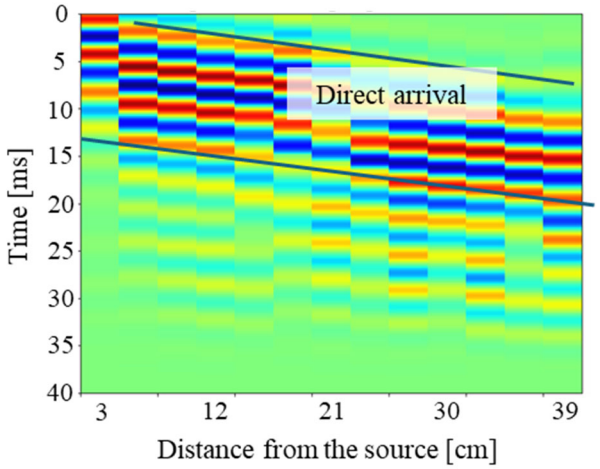

Figure 4. Time-distance waveform recorded in the homogeneous case

3 EXPERIMENTAL RESULTS

3.1 *Observation of Cavity Reflections and Refractions*

Figures (4) and (5) present cross-correlated seismograms for the homogeneous and cavity cases, respectively. In the cavity ground, direct-wave attenuation was pronounced directly above the cavity, while residual arrivals interpreted as reflections persisted between the source and cavity (up-dip side). Faster-propagating refracted waves appeared down-dip, indicating cavity-induced modifications of the wavefield.

3.2 *Surface-Wave Dispersion*

Dispersion images for the two cases are shown in Figures (6) and (7). Both display the fundamental Rayleigh-wave mode (yellow dashed lines), consistent with prototype ground when V_s is matched. A common peak with diverging phase velocity at 350–500 Hz (green dashed lines) is attributed to reflections from the box bottom (~350 mm depth) and walls.

For the cavity case, an additional high-frequency (> 500 Hz) peak (black dashed line) emerged, representing an extra dispersion mode generated by the cavity. Because the cavity roof forms a secondary free surface, boundary conditions resemble a thin plate; the resulting mode is analogous to a Lamb-type guided wave[7] confined between the ground surface and cavity roof.

3.3 *Attenuation Evaluation*

Attenuation was assessed in three zones: up-dip (in front of cavity), directly above, and down-dip. Figure (8) plots mixed-wave spectra versus distance, revealing local amplitude peaks up-dip caused by superposed reflections. Figures 9 and 10 show direct-wave spectra only. When the source was not above the cavity, as shown in Figure (9), the apparent geometric-spreading exponent was larger than up-dip, implying scattering losses into the cavity.

Even when the source straddled the cavity: Figure (10), direct-wave amplitudes decayed more rapidly above the cavity as distance increased, suggesting energy leakage into cavity-related guided waves. Because direct waves dominate total motion, their attenuation exaggerates residual vibrations above the cavity, yielding the lingering waveforms observed.

4 CONCLUSIONS

An elastic-wave experiment in a controlled sand box demonstrated the feasibility of seismic methods for detecting underground cavities. Comparing homogeneous and cavity cases revealed three key features:

1. Between the source and cavity, reflections and refractions persist after the direct wave, producing local spectral peaks in the mixed-wave Fourier amplitude upstream of the cavity.
2. In the cavity ground, a new high-frequency (> 500 Hz) dispersion peak appears in the frequency–phase-velocity domain. This higher mode arises between the ground surface and the cavity roof.
3. Direct-wave amplitudes attenuate markedly above the cavity relative to up-dip ground. When the source is cavity-centered, amplitudes above the cavity diminish more rapidly with distance than those over intact ground.

These signatures provide diagnostic criteria for seismic detection of deep-seated underground cavities, thereby enhancing early countermeasures against potential ground sinkholes.

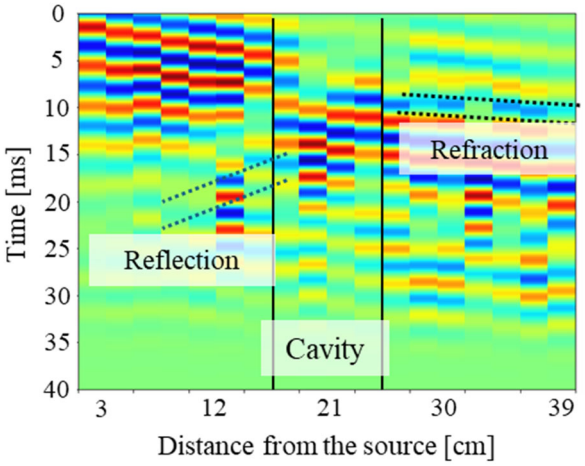

Figure 5. Time-distance waveform recorded in the cavity embedded in homogeneous ground model case. The cavity was positioned 110 mm below the surface, beneath the 15cm-27cm distance from the source.

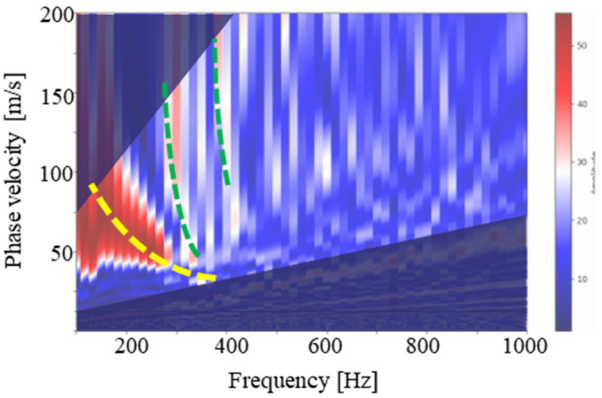

Figure 6. Dispersion relation between frequency and phase velocity in homogeneous ground model case. Yellow dashed line: fundamental mode; green dashed line: mode induced by the sand-box boundary.

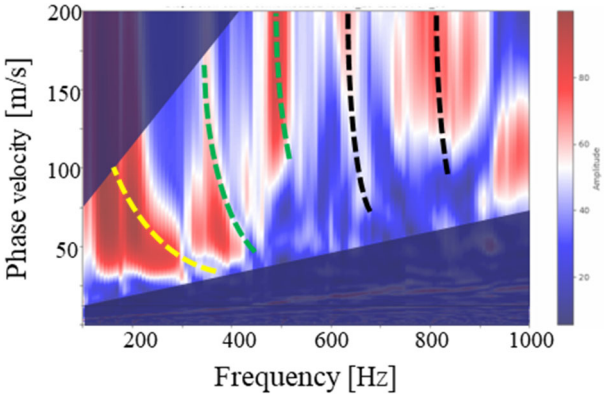

Figure 7. Dispersion relation between frequency and phase velocity in cavity-bearing ground. The peak unique to the cavity ground is denoted by black lines.

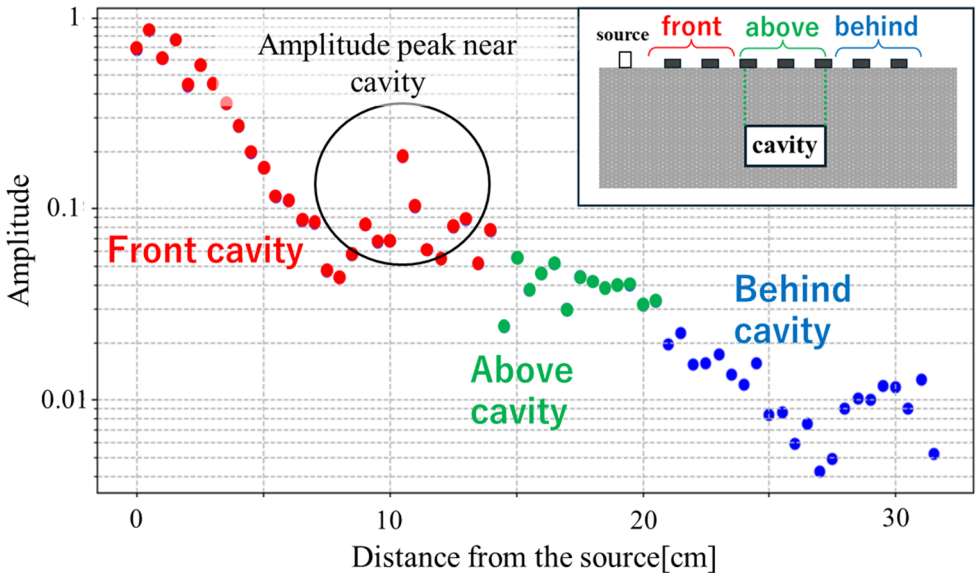

Figure 8. Relationship between propagation distance and Fourier spectrum for the direct–reflected mixed wave

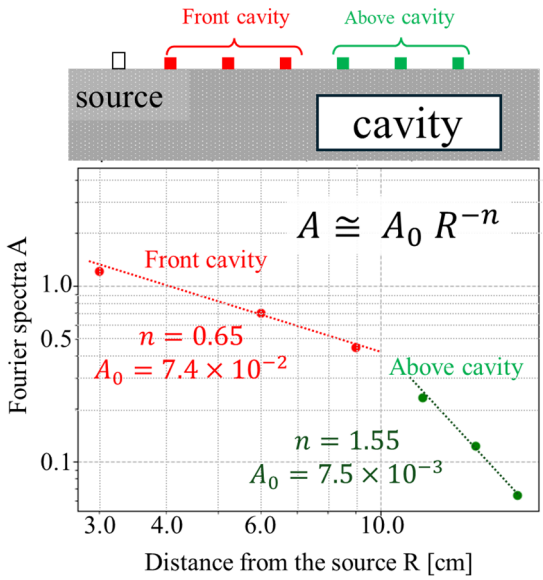

Figure 9. The relationship between direct-wave amplitude and propagation distance when the excitation source is not directly above the cavity.

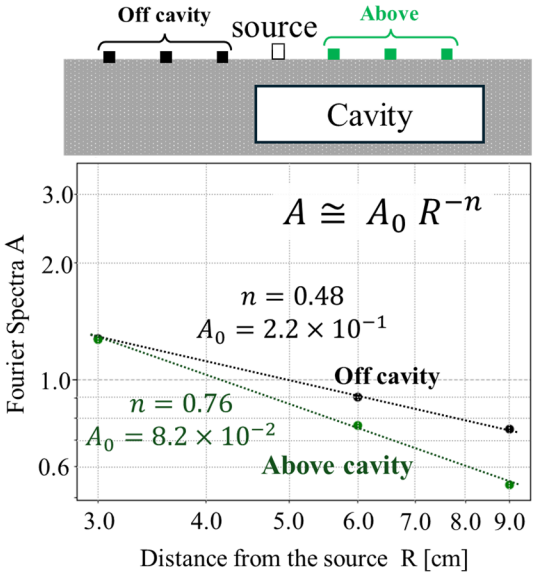

Figure 10. The relationship between direct-wave amplitude and propagation distance when the exciter is positioned directly above the cavity.

5 REFERENCES

Kuwano, R., et al. 2009. Study on the detection of underground cavity and ground loosening for the prevention of ground cave-in accident. *Japanese geotechnical journal 5(2)*, 219-229.

Kuwashiro, K. 2025. *Fundamental study for detecting deep underground cavity and loosening by shield tunneling*, Master's thesis, The University of Tokyo, Tokyo, Japan.

Karasaki, Y. 2022. *Challenge of detecting deep-ground cavities using wave propagation in soil,* Master's thesis, The University of Tokyo, Tokyo, Japan.

Tao, S., et al. 2019. Evaluation of Soil Moisture and Shear Deformation Based on Compression Wave Velocities in a Shallow Slope Surface Layer, *Sensors*, 19(15), 3406

Park, C. B., et al. 1998. Imaging dispersion curves of surface waves on multi-channel record. *SEG Technical Program Expanded Abstracts*, Kansas Geological Survey.

Bornitz, G. 1931. *Über die Ausbreitung der von Großkolbenmaschinen erzeugten Bodenschwingungen in die Tiefe*. Springer.

Lamb, H. 1917. On waves in an elastic plate. *Proceedings of the Royal Society of London, Series A* 93, 114–128.